

U. VOGT<sup>1,✉</sup>  
R. FRUEKE<sup>1</sup>  
T. WILHEIN<sup>1</sup>  
H. STOLLBERG<sup>2</sup>  
P.A.C. JANSSON<sup>2</sup>  
H.M. HERTZ<sup>2</sup>

## High-resolution spatial characterization of laser produced plasmas at soft x-ray wavelengths

<sup>1</sup> RheinAhrCampus Remagen, University of Applied Sciences Koblenz, Südallee 2, 53424 Remagen, Germany

<sup>2</sup> Biomedical and X-Ray Physics, Royal Institute of Technology/Albanova, 10691 Stockholm, Sweden

Received: 8 July 2003/Revised version: 8 September 2003

Published online: 4 November 2003 • © Springer-Verlag 2003

**ABSTRACT** In this article, we describe the setup and application of a system for the spatial characterization of laser-produced plasma x-ray sources. While pinhole cameras are normally used for this purpose, we employed a zone plate to act as the x-ray lens. Together with an x-ray CCD camera as the detector, a spatial resolution of up to 2  $\mu\text{m}$  was achieved. Due to the wavelength-dependent focal length of a zone plate, the monochromaticity of the image was better than  $\frac{\lambda}{\Delta\lambda} = 150$ , and the large aperture of the zone plate allowed single-laser-shot images to be collected. Methanol and ethanol were used as liquid-jet target systems. Two different Nd : YAG lasers with pulse durations of 3 ns and 10 ns produced the plasmas. Our measurements concentrated on the line emission of carbon in the soft x-ray spectral range, namely, the hydrogen-like  $\alpha$ -line at 3.37 nm and the helium-like  $\alpha$ -line at 4.03 nm. We investigated the influence of different nozzle sizes, laser energies, and pulse durations on the source size of the plasma. Depending on the experimental conditions, plasma diameters of 17–60  $\mu\text{m}$  were measured.

PACS 41.50.+h; 52.38.-r; 52.70.La

### 1 Introduction

The interaction of intensive laser radiation with solid, liquid, or gaseous/cluster targets has been subjected to extensive attention in the recent past because of the soft and hard x-ray radiation emitted from the created plasmas. These plasmas can be used as compact x-ray sources, and open up a laboratory operation of a variety of application experiments. Among them are x-ray microscopy [1, 2], near-edge x-ray absorption spectroscopy [3], time-resolved x-ray diffraction experiments [4], and extreme ultraviolet lithography [5], to name only a few. Many such applications require an accurate characterization of the spatial distribution of the emitted radiation. Previous techniques are hampered by low resolution, lack of spectral selectivity, and a low collection efficiency. In the present paper we demonstrate high-resolution spectral imaging using a zone plate and apply the technique to a laser plasma x-ray source.

Among the possible target systems for a laser-produced plasma, liquid jets or droplets are of special interest, since they are low-debris targets compared with solid targets [6]. This is the same for gaseous/cluster targets [7], but the advantage of a thin liquid jet with a diameter typically in the 10–30  $\mu\text{m}$  range is the small and spatially defined target volume that can lead to small source sizes on the same order of magnitude. Such small plasmas are a prerequisite for some of the above-mentioned applications.

Laboratory x-ray microscopy is such an application. At the Biomedical and X-Ray Physics division in Stockholm, a laboratory soft x-ray microscope has been set up for the water-window spectral range [2]. This wavelength region between the *K*-absorption edges of oxygen and carbon provides a natural contrast between material containing carbon on the one side and water on the other side [8]. It is therefore possible to examine biological samples like proteins in their natural aqueous environment. The optics in the microscope consist of a spherical multilayer mirror in normal incidence as the condenser and a micro zone plate as the objective. The light source is a liquid-jet target laser plasma source operating with methanol as the target liquid. The multilayer mirror images the plasma with a magnification of 1.8 $\times$  in the object plane, which typically has a 20- $\mu\text{m}$ -diameter field of view. It is clear that the source size should be in the range 10–20  $\mu\text{m}$  to lose as little radiation as possible for the illumination of the object. Therefore, a detailed analysis of the actual source size with a spatial resolution below 10  $\mu\text{m}$  should be performed. Besides the value for the source diameter the spatial intensity distribution of the emitted radiation is also of interest for a theoretical performance study of the microscope.

For the spatial emission characterization of laser-produced plasmas, the use of pinhole cameras consisting of a small aperture and a CCD detector is a standard technique [9], although this method has a series of disadvantages. It is especially unsuited to the measurement of small sources, since the pinhole size limits the resolution. Very small pinholes in the range of few microns must be used for high resolution in the 10- $\mu\text{m}$  range, so the intensity of the image is very low due to the small collected solid angle. Another drawback is the fact that the method is not wavelength selective and an image integrated over the whole spectrum is detected. In some cases, this effect can be reduced by the use of suitable bandpass filters, but in the water window, no filters exist that can separate one emis-

✉ Fax: +49-2642/932-359, E-mail: vogt@rheinahrcampus.de

sion line or a defined small wavelength region from the rest of the spectrum.

In this article we present a different method for the spatial characterization of laser-produced plasmas. We used a zone plate (ZP) as an x-ray lens to form a magnified image of the source [10, 11]. Depending on the setup, which includes the ZP designed especially for the water-window spectral range and the detector, a high spatial resolution of 2–5  $\mu\text{m}$  can be achieved. This resolution cannot be achieved with pin-hole cameras nor with other optical elements suited to the water window [12, 13]. Due to the large aperture of the ZP used, it is possible to detect an image with a single laser pulse and to investigate the source stability. Furthermore, since the focal length of the ZP is wavelength dependent, only a small wavelength region contributes to the formation of the image. All experiments were performed in the framework of source-size and intensity-distribution characterization of the laser-produced plasma used as the light source for the soft x-ray microscope and show the potential of this experimental technique. The results are also interesting for a better understanding of laser–matter interaction characteristics in the spatial domain.

## 2 High-resolution imaging with zone plates

Zone plates are circular gratings with decreasing grating constant towards the outermost zones and can be used as high-resolution x-ray optics [14]. Their focusing properties are due to diffraction; thus, the focal length  $f_{zp}$  of a ZP is wavelength dependent:

$$f_{zp}(\lambda) = \frac{2r_n \times dr_n}{m \times \lambda} \quad (1)$$

with  $r_n$  the ZP radius,  $m = \pm 1, 2, \dots$  the different diffraction orders, and  $dr_n$  the outermost zone width. Normally, a ZP is used in the +1 diffraction order. The diffraction-limited size of the focus  $\delta_{zp}$  is determined by the outermost zone width  $dr_n$ :

$$\delta_{zp} = 1.22 \times dr_n. \quad (2)$$

The ZP forms a magnified image on the CCD detector (Fig. 1). The image equation is the same as for normal lenses [15]:

$$\frac{1}{f_{zp}} = \frac{1}{g} + \frac{1}{b}. \quad (3)$$

The magnification  $M$  follows from the object distance  $g$  and the image distance  $b$ :

$$M = \frac{b}{g}. \quad (4)$$

With the help of the last two equations, the geometry of a setup for a given wavelength and desired magnification can be calculated. The magnification also influences the monochromaticity  $\frac{\lambda}{\Delta\lambda}$  of a certain setup, which can be calculated by simple geometric considerations:

$$\frac{\lambda}{\Delta\lambda} = \frac{M+1}{M} \frac{r_n}{d}. \quad (5)$$

The diameter of the source is specified by  $d$  in this equation.

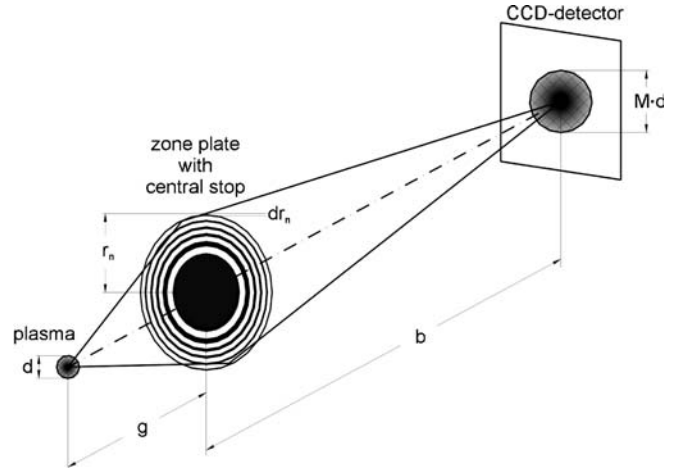


FIGURE 1 Schematic drawing of high-resolution imaging using a zone plate

The ZP used for the experiments is of the type KZP7 that originally acted as the condenser optic in the transmission soft x-ray microscope at the electron storage ring BESSY in Berlin. The KZP7 is made of germanium on a silicon substrate (a detailed description of the manufacturing process can be found in [16]) and features an outermost zone width of  $dr_n = 54 \text{ nm}$ . The diameter of the KZP7 is  $2r_n = 9 \text{ mm}$ , while in the middle area a central stop of 5 mm is applied to block the zeroth diffraction order. The relatively large ZP aperture results in a large collected solid angle and makes the system highly efficient for performing single-shot images. Another important parameter is the focal length  $f_{KZP7}$  of the KZP7 in the +1 diffraction order:

$$f_{KZP7} = 201 \text{ mm} \times \frac{2.4 \text{ nm}}{\lambda}. \quad (6)$$

From (6) it follows that  $f_{KZP7}$  in the water-window spectral region is in the range 200–110 mm. This is an almost ideal value, since the ZP must not be placed too close to the plasma to prevent its destruction due to debris but it is placed close enough to collect a large amount of the emitted radiation. The diffraction-limited resolution of the KZP7 is  $\delta_{KZP7} \approx 60 \text{ nm}$ ; however, the achievable resolution is usually limited by the pixel size of the CCD chip. At magnifications between 10 and 24, it is in the range 2–5  $\mu\text{m}$  ( $24 \times 24\text{-}\mu\text{m}^2$  pixel size), which is sufficient for the sources under investigation. For sources with diameters of 20–30  $\mu\text{m}$ , the resulting monochromaticity  $\frac{\lambda}{\Delta\lambda} = 150\text{--}230$  allows one to separate different images for different wavelengths in the detector plane if the plasma emits well-separated line radiation.

## 3 Experimental setup

The basic experimental setup of the soft x-ray source is shown in Fig. 2. Self-made glass capillary nozzles with diameters of 10–20  $\mu\text{m}$  were used to form a liquid jet in a vacuum chamber. We chose methanol as the target liquid since it contains carbon with emission lines in the water window. The chamber was evacuated with a turbo-drag pump (8801/sec) in combination with a rotary vane pump (16  $\text{m}^3/\text{h}$ ). A differential pumping stage removed the jet out

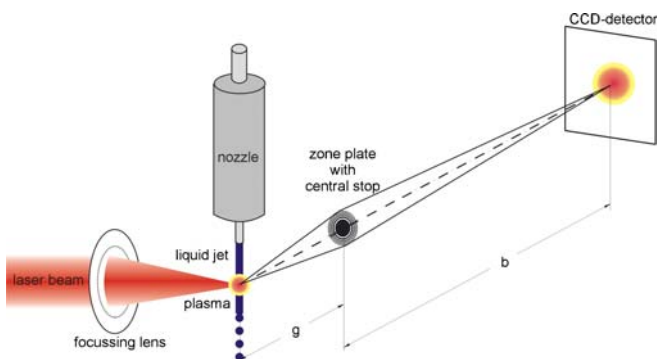


FIGURE 2 Experimental arrangement of the liquid-jet laser-plasma source

of the vacuum. During operation, a pressure of  $5 \times 10^{-3}$  mbar could be achieved in the target chamber.

A frequency-doubled Nd–YAG laser (Coherent Infinity 40-100,  $\lambda = 532$  nm) was focused on the laminar part of the jet to produce the plasma. The laser operated at a maximum repetition rate of 100 Hz and a pulse duration of 3 ns. The highest possible pulse energy is around 200 mJ; however, only energies up to 166 mJ were applied in the experiments. The laser beam was focused by a lens to a calculated spot of  $12 \mu\text{m}$  in diameter (FWHM), which resulted in a maximum intensity on the target of about  $5 \times 10^{13}$  W/cm<sup>2</sup>.

The observation direction with the ZP was in the same plane as the laser beam at an angle of 90 degrees (see Fig. 2). Due to space limitations in the laboratory, the maximum distance between the plasma and the detector could not be larger than about 2.5 m. The ZP was mounted on a 3-axis translation stage so as to be able to focus the image in the center of the CCD detector. The experiments concentrated firstly on the hydrogen-like carbon emission line Ly- $\alpha$  at 3.37 nm because the microscope worked at this specific wavelength. The focal length of the KZP7 for 3.37 nm was  $f_{3.37 \text{ nm}} = 143.1$  mm. The distances were chosen to be  $g = 153$  cm between the plasma and the ZP and  $b = 2211$  mm between the ZP and the detector, which resulted in a magnification of  $M = 13.8\times$ . A CCD camera (Photometrics AT200L) with a thinned back-illuminated chip (Tectronix 1024AB,  $1024 \times 1024$  pixels) served as a soft x-ray detector. The pixel size of  $24 \times 24 \mu\text{m}^2$  yielded a spatial resolution of  $3.5 \mu\text{m}$  in the acquired images (resolution element  $\hat{=}$  two pixels).

For the experiments described in Sect. 4.4, a slightly modified setup was used. Instead of methanol, an ethanol jet was produced by a different nozzle system that delivered jets of  $40\text{-}\mu\text{m}$  diameter. The laser beam, the jet, and the observation direction were oriented in the same plane with an angle of 30 degrees between the laser and the observation axis. The laser focus had a size of  $17 \mu\text{m}$  (FWHM). Besides the Coherent Infinity laser, a Spectra DCR-3D laser (frequency-doubled Nd : YAG) created the plasma. This laser, providing a pulse energy of 150 mJ at a wavelength of 532 nm, delivered longer laser pulses of 10 ns. By using these two laser systems, we were able to examine the influence of the pulse duration on the source size for two different carbon emission lines, Ly- $\alpha$  at 3.37 nm, as described above, and, additionally, the He- $\alpha$  line of helium-like carbon at 4.03 nm. To change the image to the latter wavelength, the plasma–detector distance was fixed and only the

ZP was moved to create a sharp image at a slightly different magnification.

#### 4 Results and discussion

Figure 3 shows an image taken at a wavelength of 3.37 nm with the  $19.4\text{-}\mu\text{m}$  nozzle and a laser energy of 163 mJ. In the center the sharp image can be clearly seen. The laser beam direction is to the right. Around this area the defocused wavelengths produce a shadow projection of the central stop that has three support stripes. Different wavelengths can be distinguished due to the different sizes of the shadows. This indicates the sufficient monochromaticity to clearly sep-

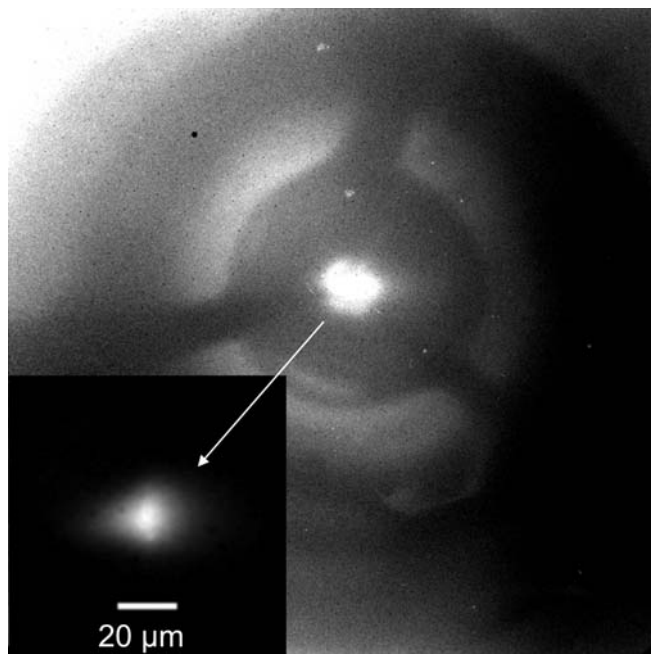


FIGURE 3 Example of an image that can be detected with the CCD camera. In the center, the focused wavelength of 3.37 nm can be seen. Around the center, the defocused wavelengths produce shadow projections of the central stop of different sizes. The *inset* shows the focused image with a different intensity scaling. The laser impinges from the left side

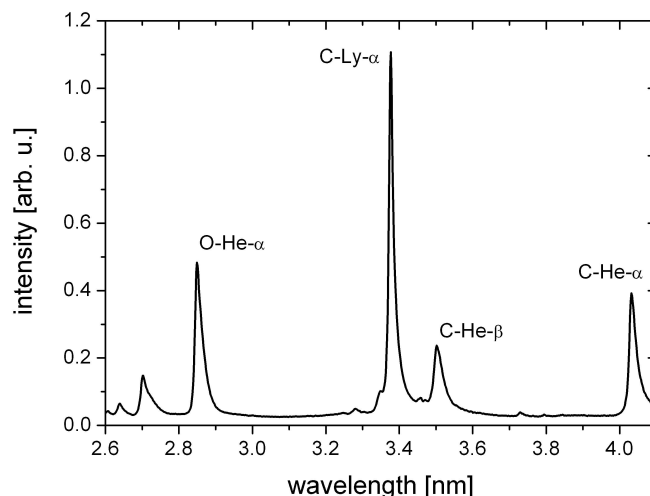


FIGURE 4 Overview spectrum in the water-window spectral range that is emitted by the plasma at a laser pulse energy of 32 mJ

arate the images of different wavelengths. Additionally, Fig. 4 shows an overview spectrum in the water-window spectral range taken with a transmission slit grating spectrograph [17]. The spectrum indicates that the level of background radiation between the single emission lines is low and should not influence the results of the plasma size measurements.

After a dark image subtraction, each plasma image was analyzed by two line plots in the horizontal and vertical directions through the pixel with the maximum intensity. As a value for the source size, the full width at half maximum (FWHM) criterion was applied. The results for different series of measurements follow in the next subsections.

#### 4.1 Influence of the jet diameter on the source size

To investigate the possible influence of the jet diameter on the source size, measurements were made at a fixed laser pulse energy of 145 mJ with three different jet diameters: 12.2  $\mu\text{m}$ , 14.2  $\mu\text{m}$ , and 19.4  $\mu\text{m}$ . Ten laser shots were accumulated in each image. Examples of resulting plots for both the horizontal and vertical directions can be seen in Fig. 5. The source size seems to be independent of the jet

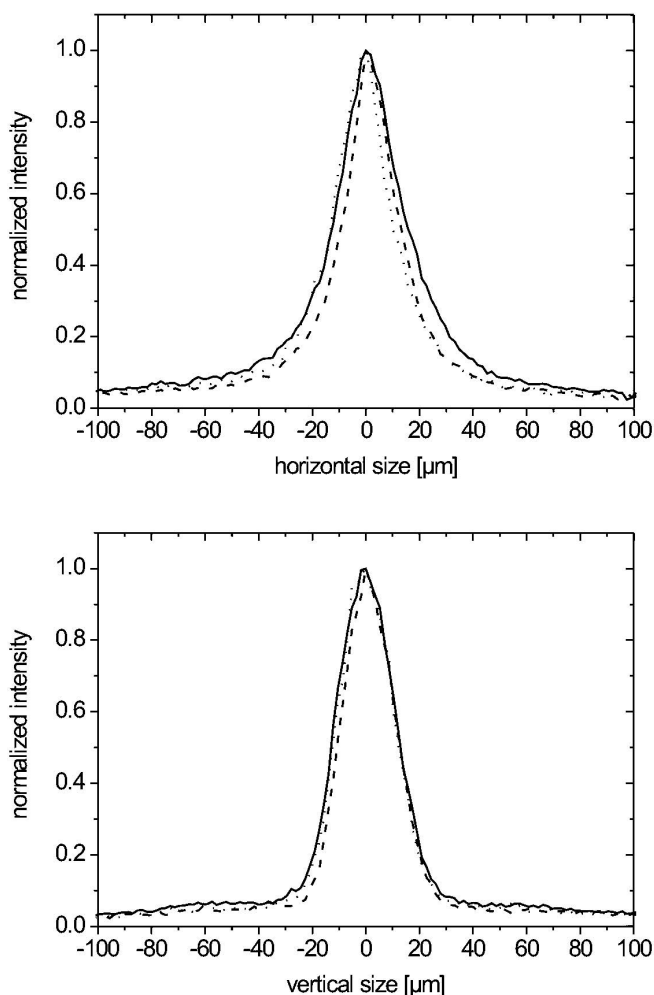


**FIGURE 5** Line plots through different images of the Ly- $\alpha$  line at a wavelength of 3.37 nm in the horizontal (*top*, laser impinging direction) and the vertical (*bottom*) direction for three nozzle diameters: 12.2  $\mu\text{m}$  (*dotted line*), 14.2  $\mu\text{m}$  (*dashed line*), and 19.4  $\mu\text{m}$  (*solid line*)

diameter. An analysis of several plots for each jet gives the following detailed results: The mean value of the horizontal size is 27  $\mu\text{m}$  for the 19.4- $\mu\text{m}$  nozzle, 26  $\mu\text{m}$  for the 14.2- $\mu\text{m}$  nozzle, and 25  $\mu\text{m}$  for the 12.2- $\mu\text{m}$  nozzle, while the mean value of the vertical size is 27  $\mu\text{m}$  for the 19.4- $\mu\text{m}$  and 14.2- $\mu\text{m}$  nozzles, and 26  $\mu\text{m}$  for the 12.2- $\mu\text{m}$  nozzle. All these values are within the resolution of the setup for 3.5  $\mu\text{m}$ , so there is no significant dependence of the plasma size on the jet size.

Within the FWHM criterion the source size seems symmetric. However, a closer look at the plots in Fig. 5 indicates that the wings of the plots in the horizontal direction are broader than in the vertical direction. This is an interesting fact because the horizontal direction is the direction of the laser beam. Since the focal depth is in the range of 450  $\mu\text{m}$ , the area in which the laser intensity is high enough to create hydrogen-like carbon ions is larger than in the vertical direction and can lead to the observed broadening of the spot in the wings.

#### 4.2 Single-shot measurements

Due to the large solid angle collected by the KZP7, it is possible to obtain single-laser-shot images of the plasma. One possibility for this is to fire only one laser shot and to expose the camera for a few seconds so that the laser shot is well within this time. The method that we applied in our experiments is different. With an open camera shutter the chip was exposed for 1 ms. After the exposure the readout of the chip was begun and during this time the laser hit the target at a frequency of 5 Hz. So during readout the chip was further exposed with the plasma images of different laser pulses. The result is that, in the completed image, each single plasma image is geometrically separated from the others. The advantage of this method is that for one image file one obtains up to 20 successive single plasma images. Figure 6 shows a part of one image with five single-shot plasmas and a line plot.

This method is ideally suited to examining both the spatial and intensity stability of the plasma emission. For the determination of the spatial stability, the size of each single-shot plasma was measured. The mean value was the same as for an image that had been integrated over several laser shots, so within the spatial resolution of 3.5  $\mu\text{m}$ , the source is spatially stable. A more unstable source would lead to a bigger integrated image size. The intensity stability follows directly from the maxima of the line plots, as shown in one example in Fig. 6. The result gives an intensity stability better than 15%.

#### 4.3 Influence of the laser energy on the source size

To investigate whether the laser energy has an influence on the source size, measurements were made with five different laser pulse energies: 166 mJ, 96 mJ, 36 mJ, 13 mJ, and 6 mJ. The nozzle diameter was 11  $\mu\text{m}$  for these experiments. The results are shown in Fig. 7. The source size decreases with decreasing laser energy. This can be qualitatively explained by the fact that an intensity variation is connected with an energy variation. However, the laser intensity has a large influence on the plasma temperature that can be reached. In the model of local thermodynamic equilibrium (LTE), the temperature determines the amount of a specific ion species that exists in the plasma. With decreasing energy and intensity the region where this temperature is high

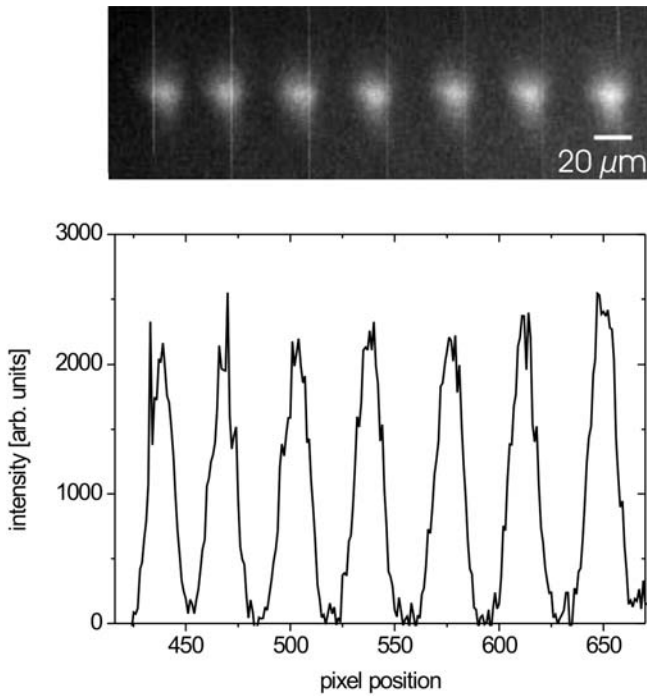


**FIGURE 6** Single-shot images at a wavelength of 3.37 nm (the white columns are CCD readout artefacts) and line plot through the center. The high spatial and intensity stability of the plasma emission is evident

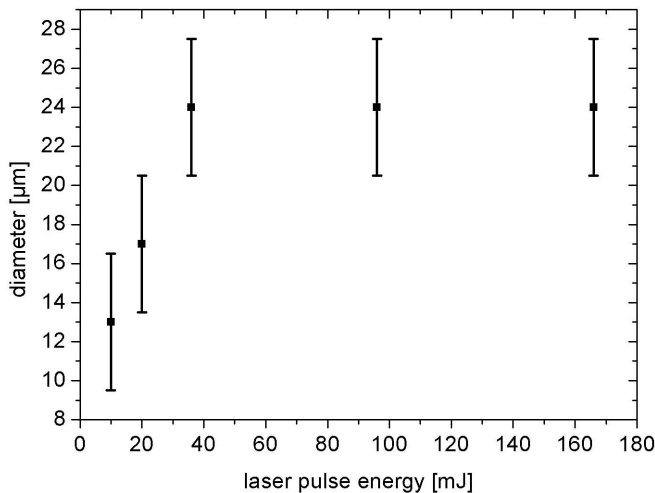


**FIGURE 7** Influence of the laser energy on the source size at a wavelength of 3.37 nm. The jet diameter was 11 μm

enough to produce hydrogen-like carbon ions also decreases and leads to a reduced source size. However, the smallest possible source size should be limited by the laser focus size, and indeed the smallest measured plasma diameter of  $13 \mu\text{m} \pm 4 \mu\text{m}$  is only slightly bigger than the laser focus.

#### 4.4 Influence of the pulse duration on the source size

As discussed in the previous section, the laser intensity has a large influence on the source size. To change the intensity, the laser energy was varied. Another possibility is the variation of the pulse duration, although in our case this means using a different laser system to produce the plasma. By using a 10-ns laser pulse, not only is the intensity changed

but the expansion dynamics of the plasma should also be affected.

We performed measurements not only at the Ly- $\alpha$  line of 3.37 nm but also at the He- $\alpha$  line of 4.03 nm to see whether the source size is different for different ion species. The images for different wavelengths and laser pulse durations can be found in Fig. 8. Additionally, the line plots in the vertical direction through the images are shown. The sizes for the Ly- $\alpha$  lines for both pulse durations and for the He- $\alpha$  line for 3 ns are nearly the same at  $22 \mu\text{m} \pm 2 \mu\text{m}$ . Only the He- $\alpha$  line for the 10-ns laser pulse is significantly larger with a value of  $60 \mu\text{m} \pm 2 \mu\text{m}$ .

A possible explanation can be found if one looks at the expansion dynamics of the plasma. The plasma expansion velocity can be calculated in terms of an isothermal expansion of a hot fluid consisting of the two species ions and electrons to be  $v_{\text{exp}} = (Z\gamma k_B T_e / M)^{1/2}$  [14], where  $Z$  is the average charge state of the plasma ions,  $\gamma$  is the adiabatic exponent,

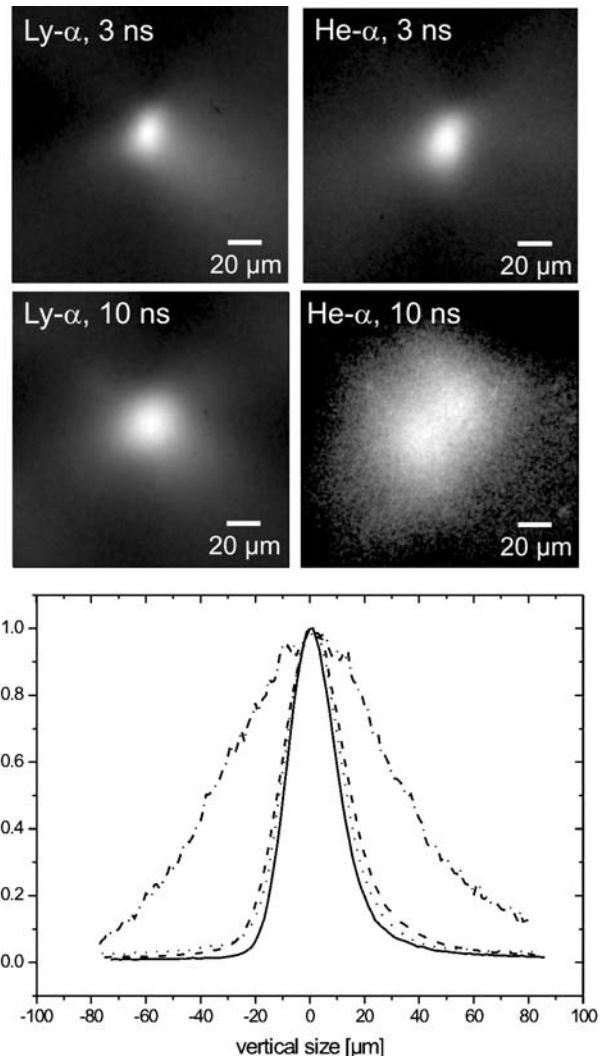


**FIGURE 8** Images of the plasma in the Ly- $\alpha$  line of 3.37 nm and the He- $\alpha$  line of 4.03 nm at two different laser pulse durations: 3 ns and 10 ns (laser impinging from the right side). The graph shows line plots through the different images in the vertical direction: 3.37 nm, 3 ns (solid line); 4.03 nm, 3 ns (dashed line); 3.37 nm, 10 ns (dotted line); 4.03 nm, 10 ns (dash-dotted line)

$k_B$  is the Boltzmann constant,  $T_e$  is the plasma temperature, and  $M$  is the ion mass. Since the intensity in the Ly- $\alpha$  line of 3.37 nm is maximum (see Fig. 4), from the LTE condition and an atomic density of  $n_i = 1.14 \times 10^{23} \text{ cm}^{-3}$  (solid state density), the plasma temperature can be estimated via the Saha–Boltzmann equation to be  $T_e \approx 100 \text{ eV}$  (maximum concentration of C-VI ions). It follows that after the immediate creation of the plasma, it begins to expand with a velocity of  $v_{\text{exp}} \approx 7.2 \times 10^4 \text{ m/s}$ , introducing an electron density gradient. During the expansion the 10-ns laser still delivers energy to the plasma that can be used to keep the plasma temperature at a certain level as a function of the local electron density. While the electron density is not high enough in a specific region to produce hydrogen-like ions, it is sufficient for helium-like ions. This could result in a larger source diameter for the He- $\alpha$  line. For a detailed investigation of the results obtained, theoretical studies are necessary that should include the time-dependent x-ray emission in combination with spatial information.

## 5 Conclusion

In conclusion, we have used a zone plate as an x-ray lens to form magnified images of laser-produced plasmas with a liquid-jet target in certain emission lines on an x-ray CCD camera. The spatial resolution of the setup was up to  $2 \mu\text{m}$ , and the large aperture of the zone plate allowed recording of single-laser-shot plasma images. As methanol or ethanol acted as the target liquid, the line emission of carbon in the water-window spectral region was investigated, especially the Ly- $\alpha$  line at 3.37 nm. With a 3-ns 163-mJ laser pulse delivered by a frequency-doubled Nd : YAG laser, the diameter of the plasma was around  $26 \mu\text{m}$  and was nearly independent of jet diameters in the range  $10\text{--}20 \mu\text{m}$ . Within a resolution of  $3.5 \mu\text{m}$ , the plasma was spatially stable, which could be verified by analyzing single-shot images. If the laser energy is reduced to below 38 mJ, the source size will also decrease because the region where the intensity is high enough to produce hydrogen-like carbon ions will become smaller. An interesting result was obtained by using a second laser with a 10-ns

pulse duration for plasma formation. While this longer pulse had no influence on the source size of the Ly- $\alpha$  line, a strong change could be observed in the He- $\alpha$  line at 4.03 nm. The plasma increased by about a factor of three to  $60 \mu\text{m}$  with a 10-ns pulse duration. This indicates that the expansion dynamics of the plasma plays an important role in the interaction of the laser pulse and the target matter.

**ACKNOWLEDGEMENTS** The authors would like to thank G. Schmahl and D. Rudolph from the Institute of X-ray Physics, University of Goettingen, for providing the zone plate KZP7.

## REFERENCES

- 1 M. Berglund, L. Rymell, M. Peuker, T. Wilhein, H.M. Hertz: *J. Microsc.* **197**, 268 (2000)
- 2 G.A. Johansson, A. Holmberg, H.M. Hertz, M. Berglund: *Rev. Sci. Instrum.* **73**, 1193 (2002)
- 3 M. Beck, H. Stiel, D. Leupold, B. Winter, D. Pop, U. Vogt, C. Spitz: *Biochim. Biophys. Acta* **1506**, 260 (2001)
- 4 T. Feurer, A. Morak, I. Uschmann, Ch. Ziener, H. Schwoerer, E. Foerster, R. Sauerbrey: *Appl. Phys. B* **72**, 15 (2001)
- 5 R. Lebert, K. Bergmann, L. Juschkin, O. Rosier, W. Neff: *Proc. SPIE* **4343**, 215 (2001)
- 6 L. Rymell, H.M. Hertz: *Opt. Commun.* **103**, 105 (1993)
- 7 H. Fiedorowicz, A. Bartnim, R. Jarocki, M. Szczurek, T. Wilhein: *Appl. Phys. B* **67**, 391 (1998)
- 8 H. Wolter: *Ann. Phys.* **10**, 94 (1952)
- 9 S. Kranzusch, C. Peth, K. Mann: *Rev. Sci. Instrum.* **74**, 969 (2003)
- 10 G. Schriever, S. Mager, A. Naweed, A. Engel, K. Bergmann, R. Lebert: *Appl. Opt.* **37**, 1243 (1998)
- 11 G. Cauchon, M. Pichet-Thomasset, R. Sauneuf, P. Dhez, M. Idir, M. Olivier, P. Troussel, J.-I. Boutin, J.-P. Le Breton: *Rev. Sci. Instrum.* **69**, 3186 (1998)
- 12 T. Wilhein, D. Altenbernd, U. Teubner, E. Foerster, R. Haessner, W. Theobald, R. Sauerbrey: *J. Opt. Soc. Am. B* **15**, 1235 (1998)
- 13 R. Lebert, G. Schriever, T. Wilhein, B. Niemann: *J. Appl. Phys.* **84**, 3419 (1998)
- 14 D. Attwood: *Soft X-Rays and Extreme Ultraviolet Radiation* (Cambridge University Press, Cambridge 1999)
- 15 M. Born, E. Wolf: *Principles of Optics* (Cambridge University Press, Cambridge 1980)
- 16 M. Hettwer, D. Rudolph: In: *X-Ray Microscopy and Spectromicroscopy* (Springer, Heidelberg 1998)
- 17 T. Wilhein, S. Rehbein, D. Hambach, M. Berglund, L. Rymell, H.M. Hertz: *Rev. Sci. Instrum.* **70**, 1694 (1999)